Highly-Efficient Impulse-Radio Ultra-Wideband Cavity-Backed Slot Antenna in Stacked Air-Filled Substrate-Integrated-Waveguide Technology

Quinten Van den Brande, *Student Member*, *IEEE*, Sam Lemey, *Member*, *IEEE*, Jan Vanfleteren, *Member*, *IEEE* and Hendrik Rogier, *Senior Member*, *IEEE*

***Abstract*—An Impulse-Radio Ultra-Wideband (IR-UWB) cavity-backed slot antenna covering the $[5.9803; 6.9989]$ GHz frequency band of the IEEE 802.15.4a-2011 standard is designed and implemented in air-filled substrate-integrated-waveguide (AFSIW) technology for localization applications with an accuracy of at least 3 cm. By relying on both frequency- and time-domain optimization, the antenna achieves excellent IR-UWB characteristics. In free-space conditions, an impedance bandwidth of 1.92 GHz (or 29.4%), a total efficiency higher than 89%, a front-to-back-ratio of at least 12.1 dB and a gain higher than 6.3 dBi are measured in the frequency domain. Furthermore, a system fidelity factor larger than 98% and a relative group delay smaller than 100 ps are measured in the time domain within the 3dB-beamwidth of the antenna. As a result, the measured time-of-arrival of a transmitted Gaussian pulse, for different angles of arrival, exhibits variations smaller than 100 ps, corresponding to a maximum distance estimation error of 3 cm. Additionally, the antenna is validated in a real-life worst-case deployment scenario, showing that its characteristics remain stable in a large variety of deployment scenarios. Finally, the difference in frequency-domain and time-domain performance is studied between the antenna implemented in AFSIW and in dielectric-filled SIW (DFSIW) technology. We conclude that DFSIW technology is less suitable for the envisaged precision IR-UWB localization application.**

***Index Terms*—Cavity-backed slot antenna, air-filled substrate-integrated-waveguide, impulse-radio ultra-wideband, high efficiency, indoor localization.**

I. Introduction

The impulse-radio ultra-wideband (IR-UWB) technology is one of the most promising solutions for accurate localization in indoor and in obstructed or difficult outdoor environments. Exploiting (sub)nanosecond duration pulses yields supreme position accuracy and ensures excellent resilience against narrowband interference and multipath effects [1], [2]. The latter adverse propagation characteristics are typically encountered in dense and heterogeneous Internet-of-Things (IoT) environments, in applications such as indoor localization [3], healthcare [4]–[8] and low-power UWB communication [9], [10].

However, the ultra-wide bandwidth of such a short pulse implies different radiowave propagation characteristics as compared to narrowband systems. Therefore, substantially different antenna topologies are required [11], exhibiting both excellent frequency- and time-domain characteristics. Moreover, UWB antenna design for practical systems should focus on guaranteeing the desired performance in the envisaged deployment scenarios, rather than being optimized in a stand-alone free-space set-up [12], [13]. On the one hand, a plethora of IR-UWB antennas are found in current literature [11], [14], [15]. These antennas exhibit suitable form factors [16] and excellent ultra-wideband characteristics. However, all these antennas were validated in stand-alone free-space conditions. They are easily detuned by objects in their direct proximity. On the other hand, [12] and [17] have proposed innovative UWB textile cavity-backed slot antennas in dielectric filled substrate-integrated-waveguide (DFSIW) technology that guarantee highly-efficient and robust performance in the frequency domain, even in the challenging IoT environment. As such, the cavity-backed slot antenna topology implemented in a dielectric substrate forms a suitable foundation to achieve the desired performance characteristics. However, the latter designs were not optimized nor validated for IR-UWB applications. Hence, to guarantee precise and robust ranging, the proposed antenna should be optimized and validated for system-oriented time-domain metrics, to account for the effect of the antenna design on the global UWB channel.

In this article, a highly-efficient IR-UWB coupled half-mode cavity-backed slot antenna in a stacked air-filled substrate-integrated-waveguide (AFSIW) technology is reported. In order to obtain the required antenna characteristics, the antenna, based on a cavity-backed slot antenna topology, is implemented using the coupled half-mode technique [18]. Furthermore, to achieve the high performance demands, as required for the precision IR-UWB localization, the antenna is realized in AFSIW technology. Through optimization in both the frequency and the time domain, the proposed antenna exhibits outstanding IR-UWB characteristics in its 3dB-beamwidth, such as a very high system fidelity factor and a minimal relative group delay. As a result, pulse distortion is minimized and time-of-arrival variations comply with the requirements for precision IR-UWB localization. For validation purposes, the antenna is also measured in a realistic hostile environment to guarantee robust ranging performance. Furthermore, the proposed antenna is suitable for mass production industrial applications owing to its low-cost fabrication process and its topology, which allows for seamless integration with the active IR-UWB electronics.

Due to the low fabrication cost and high efficiency, AFSIW technology has become a novel up-and-coming trend in microwave and millimeter wave applications [19]–[29]. Various AFSIW designs and fabrication methodologies have been proposed in literature. [19]–[23] have proposed numerous AFSIW filters, phase shifters and transitions implemented in multilayer PCB technology. Soldering paste is applied between the different milled and copper plated layers to preclude radiation leakage. Another fabrication technology is applied in [24], where an AFSIW slotted G-band horn antenna is micromachined. In [25], a 15 GHz highly-efficient AFSIW H-plane horn antenna is reported, constructed by stacking several layers of copper plated FR4 substrates. A -10 dB impedance bandwidth of 250 MHz is achieved, with a total efficiency of 89.1% at 15 GHz. In [26], a 11.75 GHz AFSIW resonant slot array is described. This design is fabricated by milling the contours of the waveguide in the dielectric substrate, after which traditional additive processes are used to metallize the milled recess. A -15 dB impedance bandwidth of 100 MHz is obtained. Finally, two AFSIW UWB antennas are reported in [27], [28]. In [27], a highly-efficient 30.5 GHz UWB AFSIW slot

Q. Van den Brande, S. Lemey and H. Rogier are with the Department of Information Technology, IDLab, Ghent University - IMEC, Technologiepark 15, 9052 Ghent, Belgium (e-mail: quinten.vandenbrande@ugent.be; sam.lemey@ugent.be; hendrik.rogier@ugent.be).

J. Vanfleteren is with the Centre for Microsystems Technology (CMST), Ghent University, Technologiepark 15, 9052 Ghent, Belgium (email: jan.vanfleteren@ugent.be).

array antenna is described, achieving a -10 dB impedance bandwidth of 2.64 GHz. In [28] a highly-efficient *Ka*-band UWB AFSIW antipodal linearly tapered slot antenna is reported, achieving a -10 dB impedance bandwidth of 14 GHz. Although both studies compare the performance of the AFSIW design to its DFSIW counterpart in the frequency domain, they are not optimized nor validated for time-domain characteristics. Hence, their use in precision IR-UWB localization applications is not recommended without further analysis.

The remainder of this paper is organized as follows. Section II outlines the antenna design process, describing the antenna specifications, the antenna topology and its operation principle, elaborating on the implementation technology and specifying the final antenna dimensions. In Section III, the AFSIW technology is compared to its DFSIW counterpart by means of simulations. The comparison is based on the antenna form factor, bandwidth performance and radiation efficiency. Finally, the simulation and measurement results for the proposed antenna are reported in Section IV. Both frequency-domain and time-domain results are discussed.

II. Coupled Half-Mode AFSIW Cavity-Backed Slot IR-UWB Antenna

A. Antenna design specifications

The proposed IR-UWB antenna is designed in compliance with the IEEE 802.15.4a-2011 standard [30]. In this work, the design is optimized for operation in the $[5.9803; 6.9989]$ GHz frequency band, covering channels 5 and 7 of the IEEE 802.15.4a-2011 standard. A magnitude of the reflection coefficient with respect to 50Ω, $|S_{11}(f)|$, below -10 dB and a total antenna efficiency of more than 85% is imposed in the entire specified frequency band.

When considering UWB antennas, time-domain effects cannot be neglected [31]. A plethora of time-domain parameters has been proposed in literature [11], but, in particular the magnitude of the relative group delay and the system fidelity factor are of importance for IR-UWB localization. The magnitude of the relative group delay [32] is considered over the frequency range of interest and is defined by

$$|\tau_{g,r}| = \left| \frac{d\phi(\omega)}{d\omega} - \frac{1}{\omega_n - \omega_0} \int_{\phi_0}^{\phi_n} d\phi \right|, \tag{1}$$

with ω and ϕ the angular frequency and phase, respectively. The system fidelity factor [33] is defined by

$$SFF = \max_t \left| \frac{\int_{t_0}^{t_n} x_1(\tau) x_2(\tau + t) d\tau}{\sqrt{\int_{t_0}^{t_n} x_1^2(\tau) d\tau \int_{t_0}^{t_n} x_2^2(\tau) d\tau}} \right|, \tag{2}$$

with $x_1(t)$ and $x_2(t)$ the input and output pulse, respectively. Furthermore, considering the envisaged application of sub-3cm accurate IR-UWB localization, the accuracy of the estimated distance is chosen as an additional system-oriented figure-of-merit. In order to minimize ranging errors to a maximum of 3 cm, the magnitude of the relative group delay $|\tau_{g,r}(f, \theta, \phi)|$ must be smaller than 100 ps and the system fidelity factor (SFF) should be higher than 98% for all orientations within the 3dB-beamwidth of the antenna [34].

Finally, antenna design for IR-UWB localization applications imposes certain requirements to guarantee robust performance and high efficiency in realistic deployment scenarios. To minimize platform and proximity effects in actual operating conditions, high shielding of the fields in undesired directions is imposed. Therefore, the radiation pattern should be tailored to the envisaged application. Furthermore, for seamless and inconspicuous integration of the IR-UWB antenna, a compact low-profile antenna design is necessary whilst maintaining a high efficiency.

B. Antenna topology

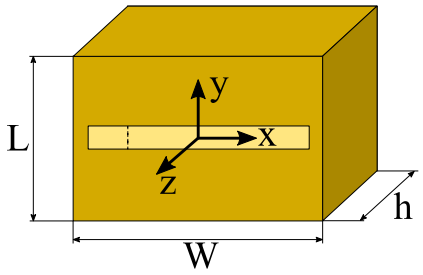

Fig. 1. Example of a conventional cavity-backed slot antenna topology.

In order to satisfy the design specifications, we rely on a cavity-backed slot antenna topology [35], as illustrated in Fig. 1, for our novel IR-UWB antenna design. It consists of a hollow metallic cavity, through which electromagnetic waves only radiate via a slot in the top metal plane. The solid metal walls confine the electromagnetic fields to the air cavity and ensure that electromagnetic radiation only originates from the slot. Thereby, the antenna mainly radiates in the hemisphere along the positive z-axis. Undesired (backside) radiation is minimized, yielding a very high front-to-back ratio (FTBR). Moreover, the topology is well-known for its very high radiation efficiency [36]. Hence, such topologies demonstrate great potential, as they provide stable characteristics when installed in or onto different everyday objects and when exploited as an integration platform for additional electronic hardware [37]. Despite these excellent features, conventional cavity-backed slot antennas mainly exhibit narrowband behavior, due to excitation of only one resonant cavity mode [38]. To enhance the bandwidth performance of the antenna, we leverage a coupled half-mode air-filled substrate-integrated-waveguide (AFSIW) cavity-backed slot antenna topology.

C. Operation principle

An ultra-wide -10-dB impedance bandwidth is obtained by judiciously combining two half-mode cavity-backed slot antennas, resonating at distinct frequencies, into one single-footprint antenna topology. The three-step design procedure is shown in Fig. 2. Two rectangular resonating cavities, operating at their fundamental TE_{110}-mode, form the starting point of the design process. Cavity A resonates at frequency f_{res1}, while cavity B resonates at frequency f_{res2}. Because of the symmetric field distribution of the TE_{110}-mode inside these rectangular cavities, their horizontal geometric symmetry plane (Fig. 2(a)) behaves as a virtual magnetic wall. Hence, in a first step, their size can be reduced by a factor two by cutting away the lower half of the cavity along this symmetry plane, without significant loss in antenna performance [39], [40]. A small ground plane extension is kept to direct radiation towards the positive z-direction. Now, both half-mode cavities radiate via leakage through the open side walls, which yields efficient antenna operation. These cavities are then brought together into one antenna topology (Fig. 2(b)), in such a way that the virtual magnetic walls of both half-mode cavities face each other, with a spacing D_{AB} between them. By removing the dielectric substrate inside the antenna, the resulting antenna forms a coupled half-mode AFSIW cavity-backed slot antenna (Fig. 2(c)).

To minimize backside radiation, as potentially generated by slots that are part of a grounded coplanar waveguide (GCPW) feed or aperture coupled feed [41], the half-mode cavity B is excited by means of a coaxial probe feed. Via the open side walls, the fields in half-mode cavity B couple into half-mode cavity A. The coupling

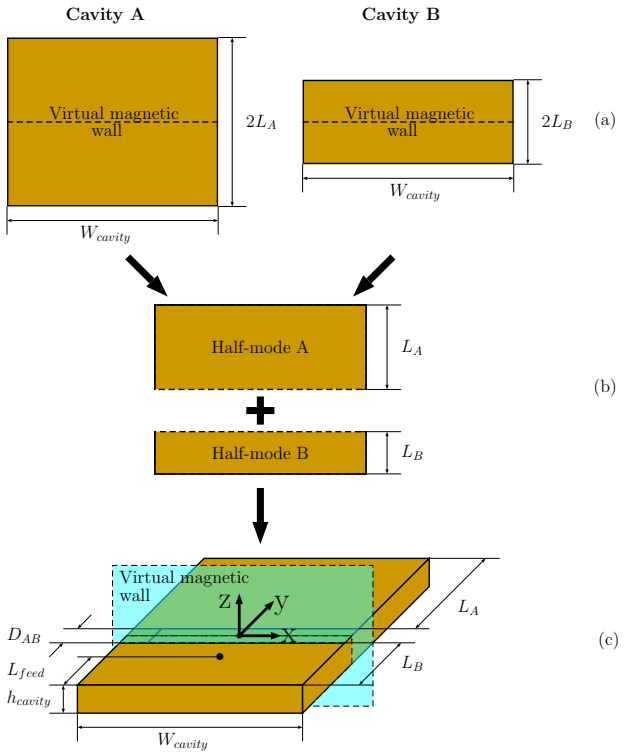

Fig. 2. Design evolution of coupled half-mode cavity-backed slot antenna.

between both half-mode cavities, controlled by the spacing D_{AB} (Fig. 2(c)) between them, introduces mode splitting [42]. As a result, the resonance frequencies of the TE_{110}-mode in the half-mode cavities shift from f_{res1} and f_{res2} to f'_{res1} and f'_{res2}, respectively. Thus, by carefully selecting D_{AB} and both resonance frequencies f_{res1} and f_{res2}, the impedance bandwidth is considerably enlarged by overlapping the -10-dB impedance bandwidth of both half-mode cavity resonances at f'_{res1} and f'_{res2}.

D. Fabrication technology

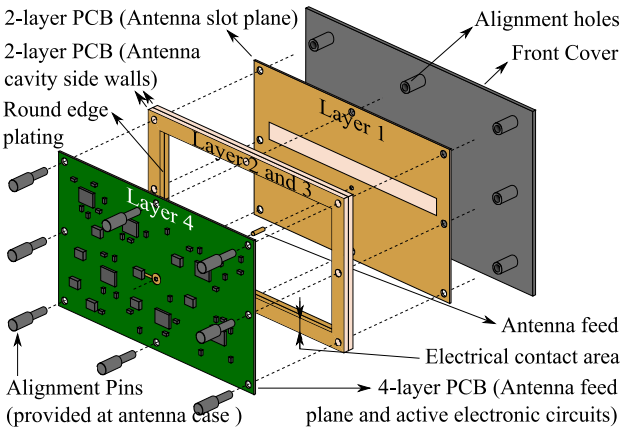

Fig. 3. Implementation of the cavity-backed slot antenna in standard PCB technology, with integrated IR-UWB circuitry. The copper plated surfaces of the antenna are indicated in dark yellow.

In this work, the coupled half-mode AFSIW cavity-backed slot antenna is realized using standard PCB manufacturing techniques in low-cost PCB substrates, as depicted in Fig. 3. The side walls of the air-filled cavity are created by milling a rectangular hole in a standard FR4 substrate [43], after which the milled sides are metalized using rounded edge plating. By relying on multiple similar FR4 substrates and/or by applying different thicknesses for each separate 2-layer PCB, a wide variety of cavity thicknesses can be obtained. Next, the feed and slot plane of the AFSIW cavity-backed slot antenna are implemented on two distinct standard PCB substrates. The antenna slot plane is implemented on a standard two-layer high-frequency laminate, such as Rogers RO4350b [44], while the antenna feed plane can be shared with the PCB on which the antenna circuitry is implemented. The latter minimizes the length of the RF connection between UWB transceiver and IR-UWB antenna. It also prevents antenna radiation from coupling into the active UWB transceiver circuitry. In order to guarantee sufficient electrical contact and to provide correct alignment between the subsequent PCB layers, alignment pins are used to tighten the boards.

E. Antenna dimensions

For the coupled half-mode AFSIW cavity-backed slot antenna, the fundamental resonant frequencies of each half-mode cavity are given by

$$f_{110} = \frac{c}{2\pi}\sqrt{\left(\frac{\pi}{W_{cavity}}\right)^2 + \left(\frac{\pi}{2L_x}\right)^2}, \tag{3}$$

with L_x the length (Fig. 2(c)) of half-mode cavity A or B [45]. In order to cover the frequency band $[5.9803; 6.9989]$ GHz, the initial resonant frequencies of the lower and upper resonant cavity are chosen to be 5.0 GHz and 8.5 GHz respectively. After frequency domain optimization in CST Design Studio for the parameters f_{res1}, f_{res2}, L_{feed} and D_{AB}, an optimal impedance bandwidth is achieved for an f_{res1} and f_{res2} of 5.172 GHz and 8.529 GHz, respectively.

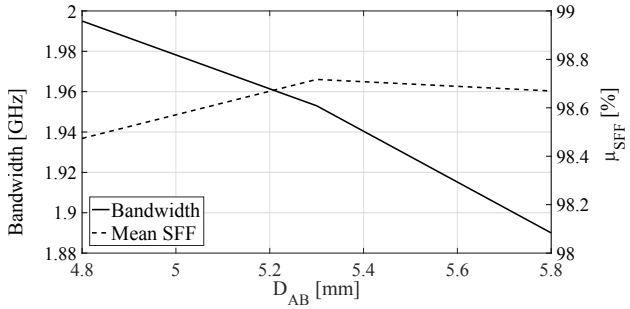

Fig. 4. Impedance bandwidth and mean system fidelity factor, μ_{SFF}, for varying slot widths D_{AB}.

A sensitivity analysis revealed that the slot width D_{AB} has a significant influence on the antenna performance in both the frequency domain and the time domain. Fig. 4 shows the -10 dB impedance bandwidth and mean system fidelity factor, μ_{SFF}, averaged over the angles of interest, for a varying slot width D_{AB}. On the one hand, it can be seen that an increase in slot width gives rise to a decrease in impedance bandwidth. On the other hand, the μ_{SFF} is maximized by setting the slot width D_{AB} to an intermediate value. Evidently, the slot width D_{AB} is an important parameter in both frequency-domain and time-domain optimization. Therefore, a multi-objective optimization is performed for the parameters D_{AB} and L_{feed}, finding the optimal point on the Pareto front, yielding the highest mean system fidelity factor for an acceptable impedance bandwidth. Furthermore, the system fidelity factor may not drop below the threshold value of 98% for all angles of interest in both channels 5 and 7, yielding an optimal slot width D_{AB} of 5.3 mm. The final antenna dimensions are given in table I. Fig. 5(a) shows a prototype of the optimized AFSIW cavity-backed slot antenna. This

TABLE I
ANTENNA DIMENSIONS FOR THE ANTENNA PROTOTYPES IMPLEMENTED IN AFSIW AND DFSIW TECHNOLOGY.

Parameter	AFSIW antenna [mm]	DFSIW antenna [mm]
W_{cavity}	41.66	30.00
L_B	9.70	6.58
L_A	20.20	10.39
H_{cavity}	3.17	4.00
D_{AB}	5.30	4.20
L_{feed}	14.90	6.39

design requires two 1.55-mm-thick FR4 PCB boards to form the copper-plated antenna side walls. An electrical contact area width of 6.00 mm was selected, as indicated in Fig. 3 and Fig. 5(a), to guarantee sufficient electrical contact between subsequent PCB-layers. Furthermore, the air gap between subsequent layers, shown in Fig. 5(b), is smaller than $10\mu m$. Simulations have shown that this gap size does not reduce the antenna performance. After assembly, the total antenna height equals 3.20 mm, because of the high-frequency RO4350b laminates on the top and bottom wall of the antenna.

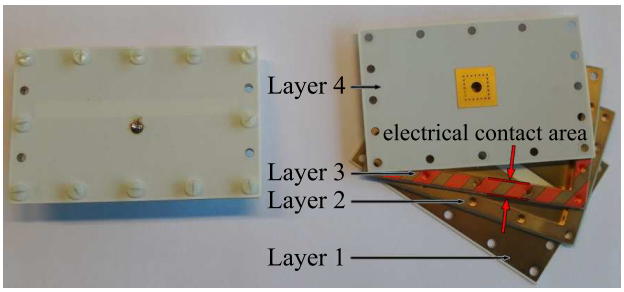

(a)

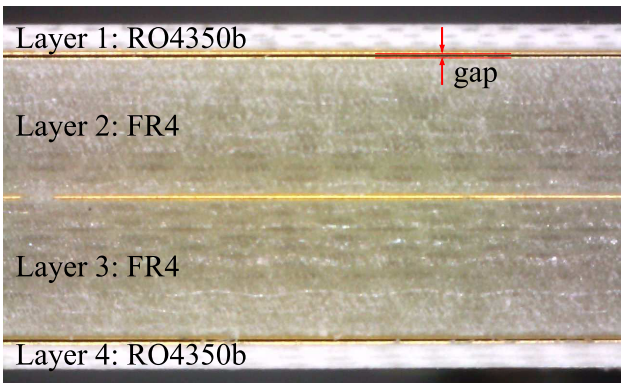

(b)

Fig. 5. Prototype of AFSIW cavity-backed slot antenna: top view (a) and side view (b).

III. AFSIW VERSUS DFSIW

For comparison, also a half-mode cavity-backed slot antenna in DFSIW technology has been designed and optimized to cover the specified frequency band of operation. The DFSIW antenna's simulation model is constructed by stacking four layers of Rogers 4350 ($\epsilon_r = 3.66$, $h_{sub} = 1.0mm$), and by applying vias with 2.00 mm diameter spaced at 3.50 mm from each other.

A. Form factor

As can be seen from table I, the dimensions of the AFSIW cavity are slightly larger than those of its DFSIW counterparts. On the one hand, the dimensions of the AFSIW cavity increase when reducing the dielectric constant of the substrate to one. On the other hand, the use of solid walls reduces the size of the AFSIW cavity compared to its DFSIW equivalent. The amount of reduction in size by the latter depends on the diameter of the vias used in the DFSIW and their spacing.

B. Bandwidth

The use of AFSIW technology, in which the dielectric substrate inside the cavity is replaced by air, induces three effects related to the antenna bandwidth performance: a decrease in electrical cavity height, being the height with respect to the wavelength, an increase of the Q-factor of both half-mode cavities and a decrease in Q of the aperture between the two half-mode cavities, mimicking the virtual magnetic wall. These effects are discussed into more depth in the remainder of this section.

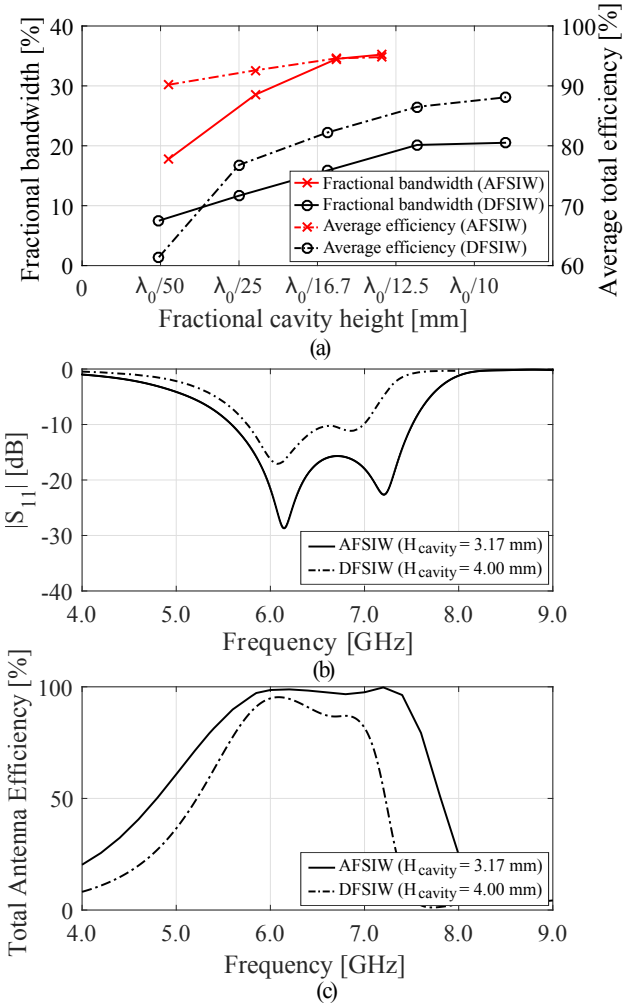

Fig. 6. Comparison between AFSIW and DFSIW cavity-backed slot antennas, based on simulation of the antennas in Table I: (a) Influence of cavity height on impedance bandwidth and total antenna efficiency. (b) Reflection coefficient w.r.t. 50Ω. (c) Total antenna efficiency.

The decrease of the electrical cavity height is a result of the increase of the effective wavelength λ_{eff}. Inherently, this lower

proportionate cavity height reduces the antenna impedance bandwidth, as specified in [38]. This effect can also be seen in Fig. 6(a), showing the relation between the fractional cavity height, $H_{cavity,frac} = H_{cavity}/\lambda_0$, with λ_0 the free-space wavelength of the center frequency, and the maximum impedance bandwidth, for both the AFSIW and DFSIW technology. Furthermore, removing the dielectric substrate inside the half-mode cavities eliminates substrate losses, results in a higher unloaded Q and a smaller impedance bandwidth. Finally, we consider the influence of the aperture on the antenna impedance bandwidth. As stated in [46], a decrease in permittivity of the substrate underneath the aperture causes a decrease of the aperture Q. Simulations with dielectric-filled half-mode cavities and an air-filled aperture have shown that the increase in bandwidth, induced by the decrease in aperture Q, is substantially greater than the decrease in bandwidth caused by the two former effects. Taking into account all effects, the impedance bandwidth is greatly enhanced by implementing the coupled half-mode cavity-backed slot antenna in AFSIW technology, as observed in Fig. 6(b).

C. Radiation efficiency

The AFSIW technology also yields a substantial improvement in radiation efficiency, compared to its DFSIW counterpart. This effect can be attributed to the following facts: a lack of dielectric losses, a reduction in ohmic losses owing to reduced surface roughness, and the absence of side wall leakage. By removing the lossy substrates, present in standard manufacturing technology, and by replacing them by air, the dielectric losses are minimized. Furthermore, [29] shows that, in case of DFSIW, the inner surface roughness of the copper foil has to be taken into account, whereas for AFSIW the outer surface roughness must be considered. As the outer surface roughness of the copper foil is smaller than the inner surface roughness, ohmic losses are reduced by implementing the antenna in AFSIW technology. Moreover, as seen in Fig. 6(a), choosing a larger cavity height, by stacking multiple sidewall layers on top of each other, reduces ohmic losses even further [47]. Finally, by using solid side walls, no electromagnetic energy can leak through the via walls used in conventional DFSIW technology, thereby significantly reducing losses and radiation in undesired directions.

Considering these improvements, the use of AFSIW technology yields a vast increase in radiation efficiency. This hypothesis is confirmed by simulation results, depicted in Fig. 6(c), showing that the DFSIW antenna reaches a maximum total efficiency of 95.36% at 6.10 GHz, whereas its AFSIW counterpart exhibits a total simulated efficiency higher than 97.0% in the complete $[5.80; 7.40]$ GHz band. Taking into account the frequency-domain limitations of the DFSIW implementation of the antenna, and because the four-layer DFSIW antenna is not poolable, leading to excessive production costs, the fabrication of a DFSIW prototype is not pursued. However, the relevant additional simulation results of the DFSIW antenna will be given in the following section.

IV. Simulation and Measurement Results

A. Frequency-domain antenna parameters

First, the antenna was measured stand-alone in an anechoic chamber. Fig. 7 shows that the simulated and measured reflection coefficients are in good agreement. Good impedance matching with respect to $Z_0 = 50\Omega$ from 5.58 GHz to 7.50 GHz can be observed, yielding a -10 dB impedance bandwidth of 1.92 GHz or 29.4%. Impedance matching in the $[5.9803; 6.9989]$ GHz band is guaranteed by implementing frequency margins of at least 300 MHz, to account for inaccuracies in the fabrication and alignment process. Fig. 8 depicts the simulated and measured total antenna efficiency, determined through the directivity/gain method [48]. It demonstrates that the total antenna efficiency is always higher than the required 85%, indicating highly efficient antenna operation. The slight discrepancy between simulation and measurement results is due to the measurement accuracy. Nonetheless, a good agreement between simulations and measurements is obtained.

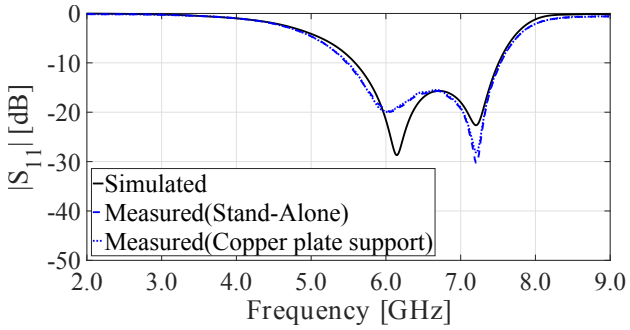

Fig. 7. Reflection coefficients w.r.t. 50 Ω of the [5.60; 7.50] GHz-band coupled half-mode AFSIW cavity-backed slot antenna, under different operating conditions.

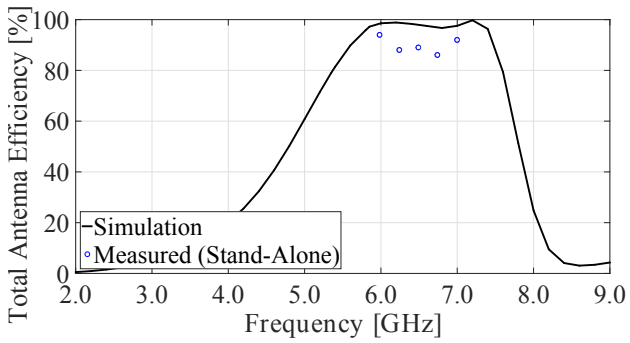

Fig. 8. Measured and simulated total antenna efficiency of the AFSIW cavity-backed slot antenna that operates in the [5.60; 7.50] GHz-band, as a function of frequency.

Fig. 9 shows the simulated and measured co- and cross-polarization radiation patterns in the azimuth (xz-plane) and elevation plane (yz-plane) of the antenna, as depicted in Fig. 2(c), at the lower, center, and upper frequency of UWB channel 7. A very good agreement between measurements and simulations is observed. This proves that our optimized design provides a gain radiation pattern that hardly changes over the desired UWB channels, thereby minimizing direction-specific distortion of UWB waveforms. The excellent antenna performance in the frequency domain is also demonstrated in Table II. Table II depicts the simulated and measured antenna gains along broadside, the FTBR, the total antenna efficiency and the 3dB-beamwidth in the azimuth and elevation plane at the three frequencies under study per UWB channel.

In addition, the antenna was measured in an anechoic chamber when mounted on a copper plate (with maximal dimensions of 35x35 cm due to weight limitations of the positioner) to mimic the worst-case deployment scenario (a perfectly conducting wall or ceiling serving as antenna platform). Fig. 7 and Fig. 9 prove that, even under such a worst-case deployment scenario, the antenna's impedance matching and radiation performance hardly changes. As a result, the total antenna efficiency also barely changes under the latter conditions. Hence, the proposed antenna provides robust, highly efficient performance in realistic deployment scenarios.

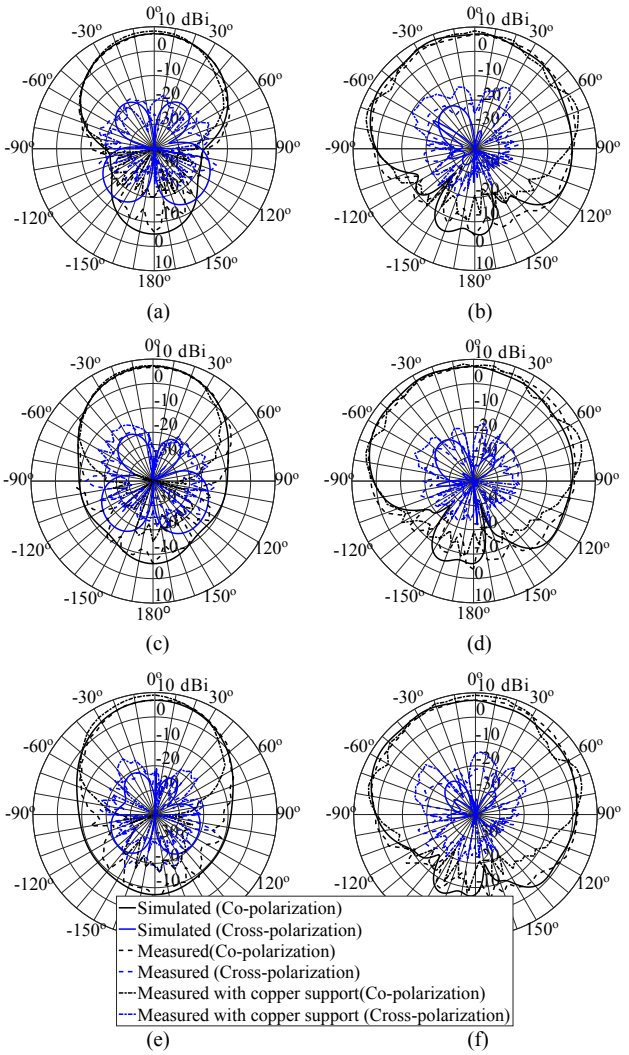

Fig. 9. Measured and simulated radiation pattern [dBi] in UWB channel 7: at 5.980 GHz in the azimuth (a) and elevation plane (b), at 6.490 GHz in the azimuth (c) and elevation plane (d), and at 6.999 GHz in the azimuth (e) and elevation plane (f).

TABLE II
SIMULATED AND MEASURED FREQUENCY-DOMAIN CHARACTERISTICS. (A) SIMULATION, (B) FREE-SPACE MEASUREMENT.

Frequency [GHz]	5.980		6.490		6.999	
	(a)	(b)	(a)	(b)	(a)	(b)
Gain [dBi]	6.9	6.9	6.8	6.3	6.9	6.6
FTBR [dB]	13.6	13.1	15.1	13.1	16.0	12.1
Antenna efficiency [%]	99.2	94.0	97.3	89.0	98.0	92.0
3 dB-beamwidth [°]						
Azimuth plane	61	55	61	65	60	60
Elevation plane	95	105	97	110	101	110

B. Time-domain antenna parameters

As stated in [31], it is imperative to consider the time-domain characteristics when designing UWB antennas. In this respect, the antenna should be analyzed in a complete transmit-receive antenna system. To this end, the coupled half-mode AFSIW cavity-backed slot antenna is used in a specific system configuration, depicted in Fig. 10, which is then measured in an anechoic chamber. To mitigate pulse distortion due to higher-order mode excitation in the coaxial measurement cables [49], high-performance coaxial measurement cables with single-mode operation up to at least 26.5 GHz were used. Furthermore, measurements are carried out in the frequency domain by performing a frequency sweep from 2 GHz to 9 GHz. In this way, the spectral content of the pulse contains no higher-order mode components after conversion to the time domain. In the setup, our coupled half-mode AFSIW or DFSIW cavity-backed slot antenna serves both as a transmit and receive antenna. In both simulations and measurements, the distance between both antennas, d, is 5.12 m. In order to analyze the relative group delay, the system fidelity factor (SFF) and the time-of-arrival (ToA) variations in the azimuth and elevation plane, the receive antenna is rotated around its x-axis ($\phi_{rx} = 0°$) and y-axis ($\phi_{rx} = 90°$), respectively. Remark that the transmit antenna always transmits along broadside, implying $\theta_{tx} = 0°$.

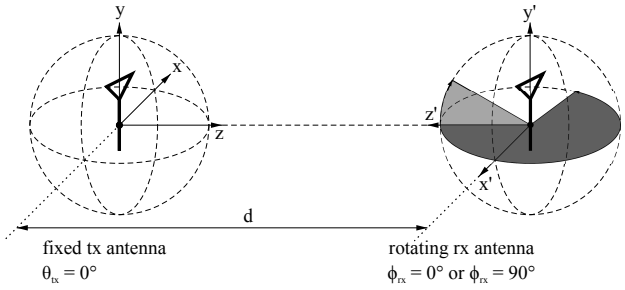

Fig. 10. System configuration for simulations and measurements with a fixed transmit (tx) antenna and rotating receive (rx) antenna.

The time-domain characterization of the antenna relies on Gaussian pulses, obtained by taking the inverse discrete Fourier transform of its Gaussian spectrum [50], defined by

$$G(f) = \frac{1}{\sigma\sqrt{2\pi}} e^{-\frac{(f-\mu)^2}{2\sigma^2}}, \tag{4}$$

with $\mu = f_{center}$ and $\sigma = \frac{BW}{\sqrt{8 \ln 10}}$. The parameters f_{center} and BW correspond to the center frequency and bandwidth of the relevant UWB channels, here channels 5 ($\mu = 6489.6$ MHz, $\sigma = 116.3$ MHz) and 7 ($\mu = 6489.6$ MHz, $\sigma = 252.0$ MHz), in the IEEE 802.15.4a-2011 standard. The pulse shapes and their positive envelope for channel 5 and 7 are depicted in Fig. 11(a) and 11(b), respectively. Each pulse is cut off after the pulse amplitude drops by 50 dB below its maximum value.

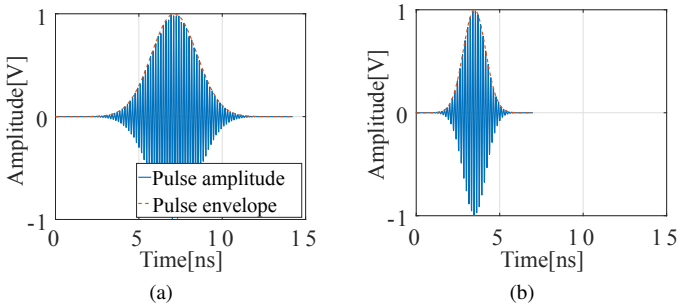

Fig. 11. Pulse shapes and their positive envelope used for time domain characterization of the antenna. (a) Channel 5. (b) Channel 7.

Fig. 12 shows the simulated and measured SFF for channels 5 and 7. When applying the 98% SFF criterion, it is found that the antenna meets the requirements in their respective 3dB-beamwidth,

as specified in Table II, indicated by the gray area in Fig. 12. Again, a very good agreement between measurements and simulations is observed. As a result, the antenna hardly introduces any pulse distortion for the Gaussian pulses in channels 5 and 7, within its 3dB-beamwidth. Furthermore, Fig. 12 also depicts the SFF for the antenna implemented in DFSIW technology. For channel 5, the DFSIW antenna complies with the 98% SFF criterion. However, for channel 7 the DFSIW antenna does not comply with the 98% SFF criterion and, hence, AFSIW technology is favored for IR-UWB localization applications.

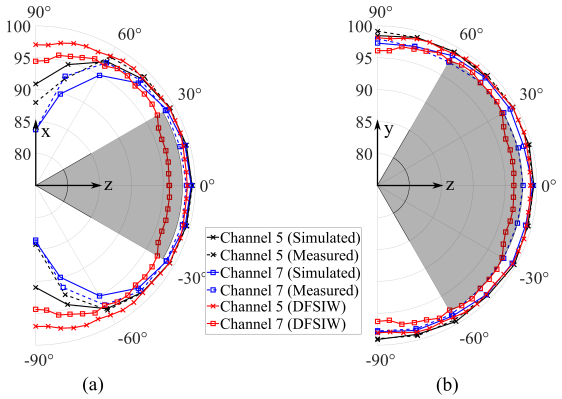

Fig. 12. SFF for the channels' 5 and 7 pulse shape in the azimuth (a) and elevation plane (b).

Fig. 13 and Fig. 14 depict the simulated and measured magnitude of the relative group delay, $|\tau_{g,r}|$, for the center and outer angle of arrival of the 3dB-beamwidth in the azimuth and elevation plane, respectively. Due to phase noise introduced by the measurement cables, a slight discrepancy can be observed between measurements and simulations. Nonetheless, we see that the antenna remains compliant with the 100 ps limitation in terms of the magnitude of the relative group delay. Both figures also depict $|\tau_{g,r}|$ for the antenna implemented in DFSIW technology. First of all, it is clear that the AFSIW antenna outperforms its DFSIW counterpart regarding the relative group delay. Furthermore, the DFSIW antenna does not comply to the 100 ps limitation in the entire frequency band of operation, and is, therefore, less suitable for IR-UWB localization applications than its ASFIW counterpart.

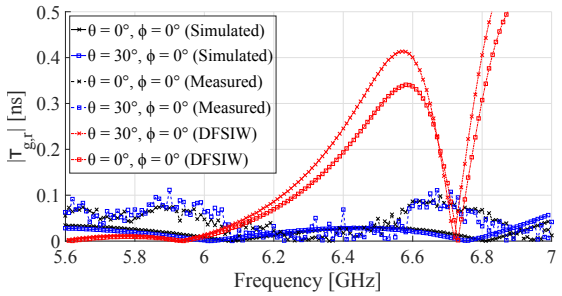

Fig. 13. $|\tau_{g,r}|$ for the coupled half-mode AFSIW and DFSIW cavity-backed slot antenna system, in the azimuth plane.

In order to verify the potential of our AFSIW antenna in precise IR-UWB ranging applications, the envelope time-of-arrival (ToA) is calculated as the time where the received pulse envelope has its maximal amplitude:

$$t_{ToA} = \arg\max |V_{rx}(t) + j\mathcal{H}\{V_{rx}(t)\}|, \tag{5}$$

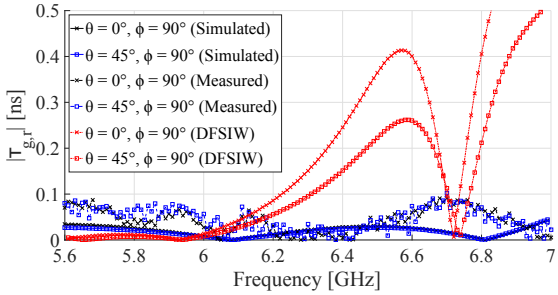

Fig. 14. $|\tau_{g,r}|$ for the coupled half-mode AFSIW and DFSIW cavity-backed slot antenna system, in the elevation plane.

with $V_{rx}(t)$ the received voltage and $\mathcal{H}$ the Hilbert transform. Fig. 15 and 16 show the simulated received voltage, as a function of time and orientation, for channels 5 and 7, respectively. The simulated and measured ToA, indicated by the solid and dashed blue line, respectively, are in good agreement. ToA variations smaller than 100 ps can be observed inside the 3dB-beamwidth of the antenna, indicating that the coupled half-mode AFSIW cavity-backed slot antenna is suitable for precise ranging applications.

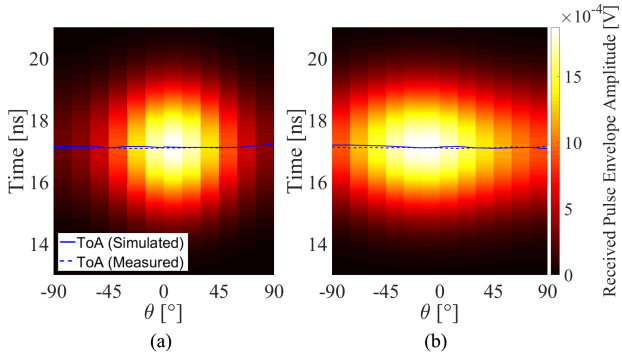

Fig. 15. Simulated and measured ToA for the coupled half-mode AFSIW cavity-backed slot antenna system, for the channel 5 pulse shape, in the azimuth (a) and elevation plane (b).

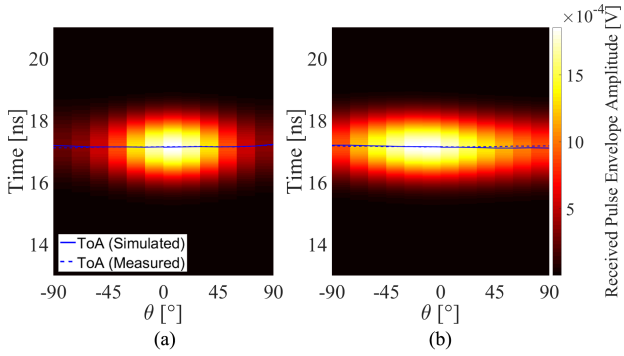

Fig. 16. Simulated and measured ToA for the coupled half-mode AFSIW cavity-backed slot antenna system, for the channel 7 pulse shape, in the azimuth (a) and elevation plane (b).

Finally, the complete system is verified in its application scenario by calculating the distance between transmit and receive antenna from the simulated and measured time-difference-of-arrival (TDoA), which is obtained by subtracting the peak time of the input pulse envelope from t_{ToA}. The estimated distance between both antennas, as a function of the angle of arrival, is depicted in Fig. 17, for channels 5 and 7. Note that noise in the measured ToA gives rise

to a small difference between the simulated and measured distance. However, both measured and simulated results yield an accuracy better than 3 cm for both channels 5 and 7 in the 3dB-beamwidth of the antenna, confirming that the coupled half-mode AFSIW cavity-backed slot antenna is suitable for precise ranging applications. Lastly, the estimated distance between the DFSIW antennas is given in Fig. 17. Although the required accuracy is achieved for both the AFSIW and DFSIW antenna within their respective 3dB-beamwidth, the ripple in the estimated distance is larger in the latter case. Hence, the AFSIW enables more accurate ranging capabilities, and is, therefore, favored for precision IR-UWB localization applications.

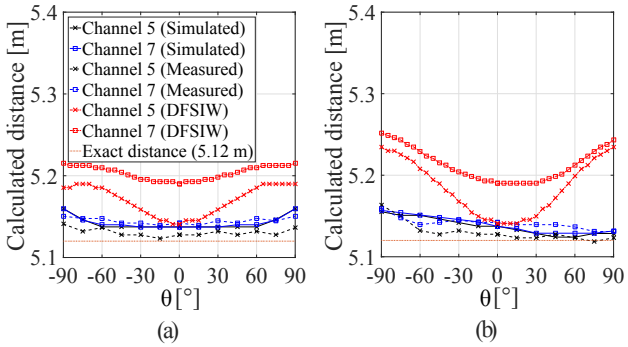

Fig. 17. Calculated distance based on simulated and measured TDoA for channels 5 and 7, in the azimuth (a) and elevation plane (b).

The excellent antenna performance in the time domain is also seen in Table III. Table III shows the simulated and measured minimal SFF within the antenna's 3dB-beamwidth, the maximum magnitude of the relative group delay and the maximum variation of the ToA within the antenna's 3dB-beamwidth.

TABLE III
SIMULATED AND MEASURED TIME-DOMAIN CHARACTERISTICS WITHIN THE ANTENNA 3DB-BEAMWIDTH. (A) SIMULATION, (B) FREE-SPACE MEASUREMENT.

	$\mathbf{SFF_{min}}$ [%]		$\lvert\tau_{g,r,max}\rvert$ [ps]		$\mathbf{\Delta ToA_{max}}$ [ps]	
	(a)	(b)	(a)	(b)	(a)	(b)
Azimuth plane						
Channel 5	99.25	99.28	57.0	110.9	40	30
Channel 7	98.69	98.42			10	20
Elevation plane						
Channel 5	99.07	99.19	44.7	102.5	60	30
Channel 7	98.73	98.03			60	20

V. CONCLUSION

A highly-efficient IR-UWB cavity-backed slot antenna implemented in stacked AFSIW technology was proposed. The design was optimized for precise localization applications operating within the IEEE 802.15.4a-2011 standard, more specifically for the channels 5 and 7, by relying on extensive frequency-domain and time-domain analysis of the antenna's characteristics.

Measurements in an anechoic chamber were performed to validate the antenna in free-space conditions in both the frequency and time domain. A very good agreement between frequency-domain simulations and measurements in terms of impedance matching and radiation performance is observed. The ultra-wide bandwidth of 1.92 GHz (29.4%) ensures coverage of both channels 5 and 7, with a maximal measured gain of 6.9 dBi and a minimal measured antenna efficiency of 89%. Furthermore, the antenna is validated in a worst-case deployment scenario. The results prove a stable antenna performance in the latter condition. Likewise, a very good agreement between time-domain simulation and measurement results is observed. A minimal SFF of 99.19% and 98.03% is measured for channel 5 and 7, respectively. The measured magnitude of the relative group delay remains lower than 100 ps in almost the complete $[5.60; 7.00]$ GHz frequency band. As a result, the estimated distance is accurate up to at least 3 cm.

Furthermore, the difference in performance between the AFSIW and DFSIW technology is studied. Simulations have shown that the use of AFSIW introduces three effects: an increase in form factor, a vast increase in impedance bandwidth and an increase in radiation efficiency. Time-domain simulations have indicated that the DFSIW is less suited for IR-UWB purposes than its AFSIW counterpart, owing to a lesser SFF and a relative group delay which is not compliant to the 100 ps criterion. In addition to its secondary performance characteristics, the fabrication cost of the DFSIW antenna is much higher than its AFSIW counterpart, because of the expensive high-frequency laminates and the non poolability of the four-layer buildup. Other low-permittivity, low-loss and low-cost high-frequency antenna foam laminates have been considered as well, such as FoamClad RF 100 [51]. Although these laminates allow for similar performance characteristics as the AFSIW technology, they are less suited mass production purposes and do not allow for integration of active IR-UWB electronics. Hence, the antenna implemented in AFSIW technology is favored for precision IR-UWB localization applications.

In conclusion, the simulations and measurements demonstrated that the antenna provides excellent IR-UWB characteristics, even in a worst-case deployment scenario. Furthermore, it is apparent that the antenna implemented in AFSIW technology outperforms its DFSIW counterpart. Hence, to achieve the required accuracy of 3 cm for localization applications the AFSIW antenna is recommended.

REFERENCES

[1] P. Meissner, E. Leitinger, M. Frohle, and K. Witrisal, "Accurate and Robust Indoor Localization Systems using Ultra-wideband Signals," in *European Navigation Conference (ENC)*, (Vienna, Austria), 23-25 Apr. 2013.

[2] W. C. Chung and D. S. Ha, "An Accurate Ultra Wideband (UWB) Ranging for Precision Asset Location," in *IEEE Int. Conf. on Ultra Wideband Systems and Technologies*, (Virginia, USA), pp. 389–393, 16-19 Nov. 2003.

[3] R. J. Fontana, E. Richley, and J. Barney, "Commercialization of an ultra wideband precision asset location system," in *IEEE Conference on Ultra Wideband Systems and Technologies, 2003*, pp. 369–373, Nov 2003.

[4] O. Novak and C. Charles, "Low-power UWB pulse generators for biomedical implants," in *2009 IEEE International Conference on Ultra-Wideband*, pp. 778–782, Sept 2009.

[5] R. Chvez-Santiago, A. Khaleghi, I. Balasingham, and T. A. Ramstad, "Architecture of an ultra wideband wireless body area network for medical applications," in *2009 2nd International Symposium on Applied Sciences in Biomedical and Communication Technologies*, pp. 1–6, Nov 2009.

[6] A. Lazaro, D. Girbau, R. Villarino, and A. Ramos, "Vital signs monitoring using impulse based UWB signal," in *2011 41st European Microwave Conference*, pp. 135–138, Oct 2011.

[7] D. T. Wisland, K. Granhaug, J. R. Pleym, N. Andersen, S. Sta, and H. A. Hjortland, "Remote monitoring of vital signs using a CMOS UWB radar transceiver," in *2016 14th IEEE International New Circuits and Systems Conference (NEWCAS)*, pp. 1–4, June 2016.

[8] J. M. Lee, J. W. Choi, and S. H. Cho, "Movement analysis during sleep using an IR-UWB radar sensor," in *2016 IEEE International Conference on Network Infrastructure and Digital Content (IC-NIDC)*, pp. 486–490, Sept 2016.

[9] J. Ryckaert, C. Desset, A. Fort, M. Badaroglu, V. D. Heyn, P. Wambacq, G. V. der Plas, S. Donnay, B. V. Poucke, and B. Gyselinckx, "Ultra-wideband transmitter for low-power wireless body area networks: design

and evaluation," *IEEE Transactions on Circuits and Systems I: Regular Papers*, vol. 52, pp. 2515–2525, Dec 2005.

[10] J. F. M. Gerrits, J. R. Farserotu, and J. R. Long, "Low-Complexity Ultra-Wide-Band Communications," *IEEE Transactions on Circuits and Systems II: Express Briefs*, vol. 55, pp. 329–333, April 2008.

[11] W. Wiesbeck, G. Adamiuk, and C. Sturm, "Basic Properties and Design Principles of UWB Antennas," *Proceedings of the IEEE*, vol. 97, pp. 372–385, Feb 2009.

[12] S. Lemey and H. Rogier, "SIW textile antennas as a novel technology for UWB RFID tags," in *2014 IEEE RFID-TA*, (Tampere, Finland), pp. 256–260, Sept. 8-9, 2014.

[13] V. Sipal, M. John, D. Neirynck, M. McLaughlin, and M. Ammann, "Advent of practical UWB localization: (R)Evolution in UWB antenna research," in *The 8th European Conference on Antennas and Propagation (EuCAP 2014)*, (The Hague, The Netherlands), pp. 1561–1565, 6-11 Apr. 2014.

[14] W. Q. Malik, C. J. Stevens, and D. J. Edwards, "Ultra-wideband Antenna Distortion Compensation," *IEEE Trans. Antennas. Propag.*, vol. 56, no. 7, pp. 1900–1907, 2008.

[15] Y. Shen and M. Z. Win, "Fundamental Limits of Wideband Localization 2014; Part I: A General Framework," *IEEE Transactions on Information Theory*, vol. 56, pp. 4956–4980, Oct 2010.

[16] G. Adamiuk, T. Zwick, and W. Wiesbeck, "UWB Antennas for Communication Systems," *Proceedings of the IEEE*, vol. 100, pp. 2308–2321, Jul 2012.

[17] O. Caytan, S. Lemey, S. Agneessens, D. Vande Ginste, P. Demeester, C. Loss, R. Salvado, and H. Rogier, "Half-Mode Substrate-Integrated-Waveguide Cavity-Backed Slot Antenna on Cork Substrate," *IEEE Antennas and Wireless Propagation Letters*, vol. 15, pp. 162–165, 2016.

[18] T. Deckmyn, S. Agneessens, A. C. F. Reniers, A. B. Smolders, M. Cauwe, D. V. Ginste, and H. Rogier, "A novel 60 ghz wideband coupled half-mode/quarter-mode substrate integrated waveguide antenna," *IEEE Transactions on Antennas and Propagation*, vol. 65, pp. 6915–6926, Dec 2017.

[19] A. Belenguer, H. Esteban, and V. E. Boria, "Novel Empty Substrate Integrated Waveguide for High-Performance Microwave Integrated Circuits," *IEEE Transactions on Microwave Theory and Techniques*, vol. 62, pp. 832–839, April 2014.

[20] J. V. Morro, A. Rodrguez, A. Belenguer, H. Esteban, and V. Boria, "Multilevel transition in empty substrate integrated waveguide," *Electronics Letters*, vol. 52, no. 18, pp. 1543–1544, 2016.

[21] A. Belenguer, J. L. Cano, H. Esteban, E. Artal, and V. E. Boria, "Empty substrate integrated waveguide technology for E plane high-frequency and high-performance circuits," *Radio Science*, vol. 52, pp. 49–69, Jan 2017.

[22] F. Parment, A. Ghiotto, T. P. Vuong, J. M. Duchamp, and K. Wu, "Ka-band compact and high-performance bandpass filter based on multilayer air-filled SIW," *Electronics Letters*, vol. 53, no. 7, pp. 486–488, 2017.

[23] F. Parment, A. Ghiotto, T. P. Vuong, J. M. Duchamp, and K. Wu, "Double Dielectric Slab-Loaded Air-Filled SIW Phase Shifters for High-Performance Millimeter-Wave Integration," *IEEE Transactions on Microwave Theory and Techniques*, vol. 64, pp. 2833–2842, Sept 2016.

[24] J. W. Digby, C. E. McIntosh, G. M. Parkhurst, B. M. Towlson, S. Hadjiloucas, J. W. Bowen, J. M. Chamberlain, R. D. Pollard, R. E. Miles, D. P. Steenson, L. S. Karatzas, N. J. Cronin, and S. R. Davies, "Fabrication and characterization of micromachined rectangular waveguide components for use at millimeter-wave and terahertz frequencies," *IEEE Transactions on Microwave Theory and Techniques*, vol. 48, pp. 1293–1302, Aug 2000.

[25] J. Mateo, A. M. Torres, A. Belenguer, and A. L. Borja, "Highly Efficient and Well-Matched Empty Substrate Integrated Waveguide H-Plane Horn Antenna," *IEEE Antennas and Wireless Propagation Letters*, vol. 15, pp. 1510–1513, 2016.

[26] F. Bigelli, D. Mencarelli, M. Farina, G. Venanzoni, P. Scalmati, C. Renghini, and A. Morini, "Design and Fabrication of a Dielectricless Substrate-Integrated Waveguide," *IEEE Transactions on Components, Packaging and Manufacturing Technology*, vol. 6, pp. 256–261, Feb 2016.

[27] F. Parment, A. Ghiotto, T. P. Vuong, J. M. Duchamp, and K. Wu, "Millimetre-wave air-filled substrate integrated waveguide slot array antenna," *Electronics Letters*, vol. 53, no. 11, pp. 704–706, 2017.

[28] A. Ghiotto, F. Parment, T. P. Vuong, and K. Wu, "Millimeter-Wave Air-Filled SIW Antipodal Linearly Tapered Slot Antenna," *IEEE Antennas and Wireless Propagation Letters*, vol. 16, pp. 768–771, 2017.

[29] F. Parment, A. Ghiotto, T. P. Vuong, J. M. Duchamp, and K. Wu, "Air-Filled Substrate Integrated Waveguide for Low-Loss and High Power-Handling Millimeter-Wave Substrate Integrated Circuits," *IEEE Transactions on Microwave Theory and Techniques*, vol. 63, pp. 1228–1238, April 2015.

[30] "IEEE Standard for Local and metropolitan area networks–Part 15.4: Low-Rate Wireless Personal Area Networks (LR-WPANs)," *IEEE Std 802.15.4-2011 (Revision of IEEE Std 802.15.4-2006)*, pp. 1–314, Sept 2011.

[31] A. Shlivinski, E. Heyman, and R. Kastner, "Antenna characterization in the time domain," *IEEE Transactions on Antennas and Propagation*, vol. 45, pp. 1140–1149, Jul 1997.

[32] D.-H. Kwon, "Effect of antenna gain and group delay variations on pulse-preserving capabilities of ultrawideband antennas," *IEEE Transactions on Antennas and Propagation*, vol. 54, pp. 2208–2215, Aug 2006.

[33] D. Lamensdorf and L. Susman, "Baseband-pulse-antenna techniques," *IEEE Antennas and Propagation Magazine*, vol. 36, pp. 20–30, Feb 1994.

[34] "APH0007 Antenna Selection / Design Guide for DW1000," tech. rep., DecaWave, 2014.

[35] J. Galejs, "Admittance of a rectangular slot which is backed by a rectangular cavity," *IEEE Transactions on Antennas and Propagation*, vol. 11, pp. 119–126, Mar 1963.

[36] G. Luo, T. Wang, and X. Zhang, "Review of Low Profile Substrate Integrated Waveguide Cavity Backed Antennas," *International Journal of Antennas and Propagation*, 2013.

[37] F. Giuppi, A. Georgiadis, A. Collado, M. Bozzi, and L. Perregrini, "Tunable SIW cavity backed active antenna oscillator," *Electronics Letters*, vol. 46, pp. 1053–1055, July 2010.

[38] G. Q. Luo, Z. F. Hu, L. X. Dong, and L. L. Sun, "Planar Slot Antenna Backed by Substrate Integrated Waveguide Cavity," *IEEE Antennas and Wireless Propagation Letters*, vol. 7, pp. 236–239, 2008.

[39] Q. Lai, C. Fumeaux, W. Hong, and R. Vahldieck, "Characterization of the Propagation Properties of the Half-Mode Substrate Integrated Waveguide," *IEEE Transactions on Microwave Theory and Techniques*, vol. 57, pp. 1996–2004, Aug 2009.

[40] I. S. S. Lima, F. Parment, A. Ghiotto, T. P. Vuong, and K. Wu, "Broadband dielectric-to-half-mode air-filled substrate integrated waveguide transition," *IEEE Microwave and Wireless Components Letters*, vol. 26, pp. 383–385, June 2016.

[41] S. S. Chakravarthy, N. Sarveshwaran, S. Sriharini, and M. Shanmugapriya, "Comparative study on different feeding techniques of rectangular patch antenna," in *2016 Thirteenth International Conference on Wireless and Optical Communications Networks (WOCN)*, pp. 1–6, July 2016.

[42] J.-S. Hong and M. J. Lancaster, "Couplings of microstrip square open-loop resonators for cross-coupled planar microwave filters," *IEEE Transactions on Microwave Theory and Techniques*, vol. 44, pp. 2099–2109, Nov 1996.

[43] "FR402 Tetrafunctional Epoxy Laminateand Prepreg," tech. rep., Isola, 2017.

[44] "RO4000 Series High Frequency Circuit Materials," tech. rep., Rogers corporation, 2017.

[45] D. Pozar, *Microwave Engineering*. Wiley, 2012.

[46] S. Yun, D. Y. Kim, and S. Nam, "Bandwidth and Efficiency Enhancement of Cavity-Backed Slot Antenna Using a Substrate Removal," *IEEE Antennas and Wireless Propagation Letters*, vol. 11, pp. 1458–1461, 2012.

[47] M. Bozzi, M. Pasian, L. Perregrini, and K. Wu, "On the losses in substrate-integrated waveguides and cavities," *International Journal of Microwave and Wireless Technologies*, vol. 1, no. 5, p. 395401, 2009.

[48] D. M. Pozar and B. Kaufman, "Comparison of three methods for the measurement of printed antenna efficiency," *IEEE Transactions on Antennas and Propagation*, vol. 36, pp. 136–139, Jan 1988.

[49] G. Wen, "A time-domain theory of waveguide," *Progress In Electromagnetics Research*, vol. 59, pp. 267–297, 2006.

[50] D. D. Wentzloff and A. P. Chandrakasan, "Gaussian pulse Generators for subbanded ultra-wideband transmitters," *IEEE Transactions on Microwave Theory and Techniques*, vol. 54, pp. 1647–1655, June 2006.

[51] "FoamClad RF 100: Low Dielectric Constant Lightweight Laminate," tech. rep., Arlon, 2003.

Quinten Van den Brande (S'17) was born in 1991. He received his M.Sc. degree in electronics engineering from Ghent University, Campus Schoonmeersen, Belgium, in 2016. He is currently pursuing the Ph.D. degree in electrical engineering with the Electromagnetics Group, Department of Information Technology, Ghent, Belgium.

His current research interests include ultra-wideband antenna design for indoor ranging systems and novel fabrication techniques for highly cost-effective antennas.

Sam Lemey (S'14 - M'16) received the M.Sc. degree in electronic engineering from Howest, University College West Flanders, Kortrijk, Belgium, in 2012 and the Ph.D. degree in electrical engineering from Ghent University, Ghent, Belgium, in 2016. He is currently working as a Post-Doctoral researcher at the Electromagnetics Group in the Department of Information Technology (INTEC) at Ghent University.

His research focuses on robust antenna systems for wearable applications, energy-harvesting techniques for wireless nodes, active antenna design for the Internet of Things and 5G applications, IR-UWB antenna systems for centimeter-precision localization, novel techniques to implement substrate integrated waveguide structures in unconventional materials, and full-wave/circuit co-optimization frameworks to realize active antenna systems.

Dr. Lemey received the Best Paper Award at the 2016 IEEE MTT-S Topical Conference on Wireless Sensors and Sensor Networks.

Jan Vanfleteren (M'00) received the Ph.D. degree in electronic engineering from Ghent University, Ghent, Belgium, in 1987.

He is currently a principal member of technical staff with the Center for Microsystems Technology (CMST) of imec, the lnteruniversity Microelectronics Centre, based in Leuven, Belgium. Jan Vanfleteren is involved in the development of novel interconnection, assembly, and polymer microsystem technologies, especially for wearable and implantable electronics, biomedical, microfluidics, cell culturing, and tissue engineering applications. ln 2004, he became a part-time Professor with Ghent University. He is the co-author of over 200 papers in international journals and conferences. He holds 17 patents and patent applications. He is a member of IEEE, IMAPS and MRS.

Hendrik Rogier (SM'06) was born in 1971. He received the M.Sc. and Ph.D. degrees in Electrical Engineering from Ghent University, Gent, Belgium, in 1994 and in 1999, respectively. He is a currently a Full Professor with the Department of Information Technology of Ghent University, Belgium, Guest Professor at imec, Ghent, Belgium, and Visiting Professor at the University of Buckingham, UK. From October 2003 to April 2004, he was a Visiting Scientist at the Mobile Communications Group of Vienna University of Technology. He authored and coauthored more than 140 papers in international journals and more than 160 contributions in conference proceedings. He is serving as an Associate Editor of IET Electronics Letters, of IET Microwaves, Antennas and Propagation, and of the IEEE Transactions on Microwave Theory and Techniques. He acts as the URSI Commission B representative for Belgium. Within the IEEE Microwave Theory and Techniques Society, he is a member of Technical Committee 24 on RFID technology and within the European Microwave Association, he is a member of the Governing Board of Topical Group MAGEO on Microwaves in Agriculture, Environment and Earth Observation. His current research interests are antenna systems, radiowave propagation, body-centric communication, numerical electromagnetics, electromagnetic compatibility and power/signal integrity.

Dr. Rogier was twice awarded the URSI Young Scientist Award, at the 2001 URSI Symposium on Electromagnetic Theory and at the 2002 URSI General Assembly. In addition, he received the 2014 Premium Award for Best Paper in IET Electronics Letters, the Best Paper Award 1st place 2016 IEEE MTT-S Topical Conference on Wireless Sensors and Sensor Networks (WiSNet), the Best Poster Paper Award at the 2012 IEEE Electrical Design of Advanced Packaging and Systems Symposium (EDAPS), the Best Paper Award at the 2013 IEEE Workshop on Signal and Power Integrity (SPI) and the Joseph Morrissey Memorial Award for the First best scientific paper at BioEM 2013. He is a Senior Member of the IEEE.